



Structure and elemental composition of Ceftriaxone induced pediatric nephrolithiasis

Yuan Du¹ · Misun Kang² · Jorge Mena³ · Marshall L. Stoller³ · Sunita P. Ho^{2,3} · Jun Li¹

Received: 12 August 2020 / Accepted: 14 November 2020
© Springer-Verlag GmbH Germany, part of Springer Nature 2021

Abstract

Ceftriaxone is a widely used antibiotic because to its broad-spectrum gram-negative coverage, safety, and biological half life (5–9 h) permit dose once-daily administration. It is specifically used in pediatric patients in developing countries. Ceftriaxone forms insoluble sludge/stone when combined with calcium in the urinary system. In this study, Ceftriaxone induced sludge/stones from pediatric patients were collected to identify its microstructure and composition to gather insights into the mechanism of Ceftriaxone induced sludge/stone formation. The results illustrated that Ceftriaxone induced stones formed rapidly following antibiotic administration. Ceftriaxone calcium salt crystals could easily be broken with minimal intervention. However, Ceftriaxone combined with calcium phosphate formed an insoluble stone aggregate.

Keywords Ceftriaxone · Nephrolithiasis · Pediatric · Calculus · Kidney

Introduction

Ceftriaxone, a third-generation cephalosporin with broad-spectrum gram-negative coverage is a commonly used antibiotic in pediatric patients, especially due to its safety and prolonged biological half life (5–9 h). The vast majority (67%) of administrated Ceftriaxone is excreted in urine [1]; the remaining drug is excreted through the biliary system. The solubility of Ceftriaxone, however, decreases when

combined with calcium, and thus can form urinary stones [2].

Ceftriaxone induced stones are rarely reported. Ceftriaxone can form sludge/stone in both the biliary (gallbladder) and urinary systems. Ceftriaxone calcium salt sludge formation has been studied in vitro with artificial urine or calcium chloride solution in distilled water [3]. The mechanism of Ceftriaxone calcium salt stone formation however remains unclear. Ceftriaxone calcium salt sludge aggregation with a rapid growth rate is an essential prerequisite to stone formation. In urologic interventions, Ceftriaxone calcium salt sludge is more commonly observed. In this study, structure and elemental compositions of Ceftriaxone induced sludge and intact stones were analyzed to gather insights into the mechanism of stone formation. The structures of sludge/stones obtained from patients were compared with calcium Ceftriaxone crystals in vitro. It is hypothesized that the structural and elemental analyses provide evidence that calcium phosphate promotes aggregation of Ceftriaxone calcium sludge and consequently forms Ceftriaxone stones.

Materials and methods

A. Surgical retrieval of Ceftriaxone stone

Protocols were approved by the ethics committee of Beijing Friendship Hospital (No. 2015-P2-012-01). All

✉ Marshall L. Stoller
Marshall.Stoller@ucsf.edu

✉ Sunita P. Ho
Sunita.Ho@ucsf.edu
https://sunholab.ucsf.edu

✉ Jun Li
lljun@yeah.net

¹ Department of Urology, Beijing Friendship Hospital, Capital Medical University, 95 Yong An Road, Xi Cheng District, Beijing 100050, China

² Division of Preclinical Education, Biomaterials and Engineering, School of Dentistry, University of California, 707 Parnassus Avenue, D 3212, San Francisco, CA 94143, USA

³ Department of Urology, School of Medicine, University of California, 400 Parnassus Avenue, San Francisco, CA 94143-0330, USA

methods were conducted in accordance with guidelines and regulations of the approved protocol. Five pediatric urinary Ceftriaxone sludge/stone specimens were obtained from five patients that either spontaneously passed the stones or were retrieved with transurethral 4.5/6.5Fr semi-rigid ureteroscopy manipulation. A guidewire was advanced, and was repeatedly moved up and down to loosen or break the sludge/stone during ureteroscopy manipulation. Poststone manipulation was performed by placing a double J stent over a guidewire and into the renal pelvis, passing the previous obstruction site where the stone was lodged. The double J stent was removed in a routine fashion 2–4 weeks after Ceftriaxone sludge/stone manipulation. Pediatric calcium oxalate and adult calcium phosphate stones were also collected during percutaneous nephrolithotomy procedure to compare their structure and elemental composition with those of Ceftriaxone stone.

The anatomical location of Ceftriaxone stone and the size of the stone were documented preoperatively by noncontrast helical clinical CT scans. Patient characteristics including age, gender, comorbidities, and hospital course were recorded. Routine stone composition was analyzed by Fourier transform infrared spectroscopy (FTIR; LIIR type, Lambda, China) to determine predominant stone components after specimen collection.

B. In vitro calcium Ceftriaxone crystal formation

Calcium chloride (CaCl₂, C1016, Sigma, St. Louis, MO) and Ceftriaxone sodium (Rocephin for injection, Roche) were used without further purification. All solutions were prepared using deionized water. Calcium chloride and Ceftriaxone sodium solutions were mixed with 1:1 molar ratio. The mixed solution was dried on a glass slide in an incubator at 37 °C.

C. Mineral density and structure analyses of stones with micro-X-ray computed tomography (micro-CT)

Intact stone specimens were scanned at 40 kVp peak voltage and at 4X magnification using micro-X-ray computed tomography (Micro-XCT 200, Carl Zeiss Microscopy, Pleasanton, California). Mineral densities were calculated following a detailed calibration protocol of the micro-CT [4, 5]. Mineral density analyses were undertaken using AVIZO[®] software (9.0.2, FEI, Hillsboro, Oregon). Higher and lower mineral density regions were segmented using intensity-based contrast algorithm.

D. Scanning electron microscopy and energy-dispersive X-ray spectroscopy

Stone specimens were embedded in LR-white resin (Electron Microscopy Science, Hatfield, Pennsylvania) and cut into two halves along the long-axis of the stone using a slow-speed saw (Isomet, Buehler, Lake Bluff, Illinois). The cut surfaces were polished using silicon carbide grit paper (sizes 800, 1200, Carbimet Paper Strips, Buehler

Ltd, Lake Bluff, IL, USA) [6, 7]. They were then imaged with micro-CT, stereo light microscope (BX51, Olympus Scientific Solutions Americas Corp. Waltham, MA, USA) and a field emission scanning electron microscope (SEM) at 1.0KeV (Sigma VP 500, Carl Zeiss Microscopy, Pleasanton, CA, USA) to visualize and compare different structures at various magnifications. Elemental composition was analyzed with energy-dispersive X-ray spectroscopy (Bruker Nano Inc., Madison, WI., USA) at an energy of 15 keV.

E. X-ray absorption spectroscopy (XAS) and X-ray fluorescence spectroscopy microprobe (XRF)

Elemental maps and sulfur K-edge X-ray absorption spectra were collected using a Vortex silicon drift detector at beamline 14–3 at the Stanford Synchrotron Radiation Laboratory. The energy scale was calibrated with reference to the energy peak of the sodium thiosulfate standard.

Sectioned stone specimens were placed inside an ion-filled chamber. Elemental maps of phosphorus and sulfur were collected at 2.5 keV. Sulfur K-edge X-ray absorption spectra were acquired from selected regions with different sulfur intensities in the specimen with a beam size of ~5 × 5 μm. Spectra corresponding to higher, medium, and lower sulfur contents were collected.

X-ray fluorescence data were analyzed using Sam's Microanalysis Toolkit (SMAK). Sulfur K-edge X-ray absorption spectra were normalized and averaged using SIXPACK data processing software.

Results

A. Ceftriaxone stone surgical intervention and outcome

Ceftriaxone stones were extracted from five pediatric patients (male:4; female:1). Patient age ranged from 6-months to 13 years. Each patient had a short history of Ceftriaxone treatment prior to acute onset of Ceftriaxone sludge/stone. Ceftriaxone, in general is used to treat pneumonia, dermatomyositis with pneumonia, lymphadenitis, postspinal nerve root resection and postcircumcision (Table 1).

Ceftriaxone was used from 3 to 7 days. Patients were presented with unilateral stones ($n=2$) while others presented in a bilateral fashion ($n=3$). Acute renal failure developed within three days after the use of Ceftriaxone in one patient (Table 1). A representative noncontrast helical computed tomography scans of a 6-month male pediatric patient revealed bilateral nephrolithiasis (Fig. 1a). The value of a nonenhanced CT Ceftriaxone induced stone image in our data was about 191–251 Hounsfield units. A representative

Table 1 Clinical information for patients administered with Ceftriaxone

Gender	Age (month)	Diagnosis and cause for medication	Ceftriaxone treatment(days)	Clinical symptoms	Stone location	Stone size(cm)
Male	6	Pneumonia	4	Anuria, renal colic	Bilateral kidney, Left ureter	0.2–0.5
Female	24	Pneumonia/Dermatomyositis	5	renal colic	Left ureter	0.3
Male	49	Postspinal nerve root resection	7	Anuria SCr:200umol/L	Bilateral ureter	–
Male	146	Acute lymphadenitis	6	renal colic, abdominal pain	Right ureter	0.5
Male	159	Postcircumcision	3	Anuria renal colic, acute renal failure SCr:663umol/L	Bilateral ureter	–

(–): Limited resolution and unable to retrieve stone size data in noncontrast helical computed tomography report

SCr Serum Creatinine

transverse CT image of a 2-year old patient revealed a left ureter stone resulting in severe hydronephrosis (Fig. 1b). Free floating sludge in the bladder was identified during cystoscopy in all cases (Fig. 1c–i) and became more pronounced after guidewire manipulation and double J-stent insertion (Fig. 1). Stone/sludge specimens were dried prior to FTIR analyses; Ceftriaxone was identified in all specimens (Fig. 1d). Double J stents were removed 2–4 weeks after stone manipulation. Renal function was within normal level in all cases with an one-year follow-up.

B. Structural and mineral density analyses of Ceftriaxone stone in comparison with pediatric calcium oxalate and adult calcium phosphate stones

Stone shape, structure, and color of Ceftriaxone stones were markedly different compared to calcium oxalate and calcium phosphate stones when viewed with a light microscope. Ceftriaxone stones were uniquely pink, with rough surfaces and multiple voids were observed within its structure. Markedly increased internal voids were appreciated with micro-CT images when compared to pediatric calcium oxalate and adult calcium phosphate stones (Fig. 2a–f). Average mineral densities of Ceftriaxone, calcium oxalate, and calcium phosphate stones were 423 ± 122 , 1274 ± 95 , 2005 ± 187 mg/cc, respectively. On average, the mineral density of Ceftriaxone stones was lower, but contained ring-like regions of higher mineral densities (650–1000 mg/cc) specifically closer to the stone surface [Fig. 2d].

C. Structural analysis using scanning electron microscopy (SEM) and elemental analysis using an energy-dispersive X-ray spectroscopy (EDX)

Ceftriaxone stone structure was fragile. Numerous spherical structures from 60 to 100 μm in diameter were seen on

the surface (Fig. 3a). A large number of honeycomb-like structures also were observed between these spheres; the honeycomb structures were radially oriented (Fig. 3b). By correlating electron and X-ray micrographs, smaller spheroidal structures (diameter $\sim 2 \mu\text{m}$) were observed in the higher mineral density regions of the Ceftriaxone stone. These spherical structures were observed in the vicinity of honeycomb structures all of which were integral to the internal architecture of Ceftriaxone stones (Fig. 3c).

Hemispherical mineral (Fig. 4) structures contained higher levels of carbon and sulfur, and lower levels of oxygen and calcium. No sodium was observed. The atomic percentage ratio of sulfur to calcium was about 2.5:1 (Fig. 4a). Carbon and oxygen components in the honeycomb areas (Fig. 3b) were similar to those found in the hemispherical mineral. The sulfur to calcium ratio, however, was increased to a ratio of 3.2:1 (Fig. 4b). The higher mineral density regions (Fig. 3c) containing the very small spherical minerals had higher phosphorus, and ratio of sulfur to calcium was reduced to 1:7.1. Interestingly, in this region the calcium atomic percentage was elevated to 10.14 compared to hemispherical regions (Fig. 4a) at 2.51 and arrow-like regions (Fig. 4b) with 2.98. The calcium and phosphorus ratio was 1.68:1, which is close to the Ca/P atomic ratio of hydroxyapatite (Fig. 4c).

D. Sulfur and phosphorus maps using microprobe X-ray fluorescence spectroscopy

Sulfur and phosphorus maps using XRF microprobe illustrated different spatial distributions of sulfur (intensity ranges: 0–1793) and phosphorus (0–203) within a stone [Fig. 5a]. Higher intensity of sulfur region was segmented using a threshold value > 1000 counts (Fig. 5b, c). Higher intensity of phosphorus region was segmented using threshold values > 50 counts (Fig. 5b, c). XAS spectra at three

Fig. 1 Clinical and chemical characteristics of Ceftriaxone stones. **a** Coronal and X-ray tomograms (left and middle), and volume rendered 3D image reconstructed (right) from X-ray tomograms of a 6-month male infant; white boxes reveal a stone in the right kidney and multiple stones in left kidney. **b** X-ray tomograms of female toddler with left hydronephrosis associated with an occluded upper ureteral stone. **c** Endoscopic images. Note the presence of floating sludge in the bladder (C-I). Inserted guide wires can be seen in the right ureteral orifice (C-II). Inserted stent can be seen in right ureter (C-III). **d** Fourier transform infrared spectrum of Ceftriaxone stone is shown

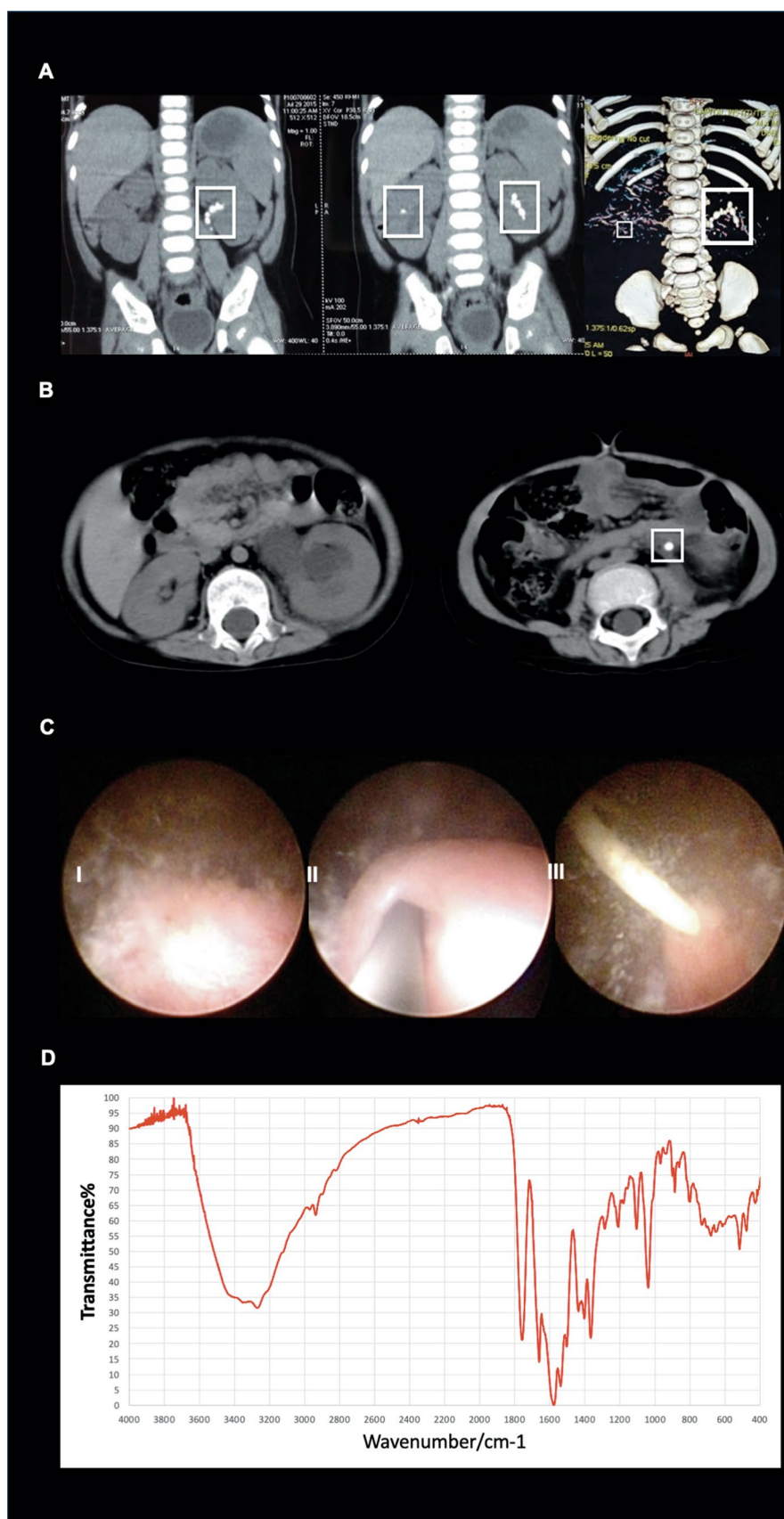


Fig. 2 Structural and mineral density analyses of Ceftriaxone in comparison with calcium oxalate and calcium phosphate stones. **a–c** Light microscopy of intact (left) and cross section (right) of Ceftriaxone, calcium oxalate, and calcium phosphate specimens are shown. **d–f** Cross sections of Ceftriaxone, calcium oxalate, and calcium phosphate stones illustrate the mineral density variation (Ceftriaxone: 0 to 1000 mg/cc; calcium oxalate: 0 to 2500 mg/cc; calcium phosphate: 0 to 3000 mg/cc) that corresponds to black to grey to white regions (left). Segmented mineral density regions of lower (Ceftriaxone: blue, 150–650 mg/cc; calcium oxalate: 300–1400 mg/cc; calcium phosphate: 300–1600 mg/cc) and higher (Ceftriaxone: red, 650–1000 mg/cc; calcium oxalate: 1400–2500 mg/cc; calcium phosphate: 1600–3089 mg/cc) ranges are shown in representative CT-slices from respective stones (right)

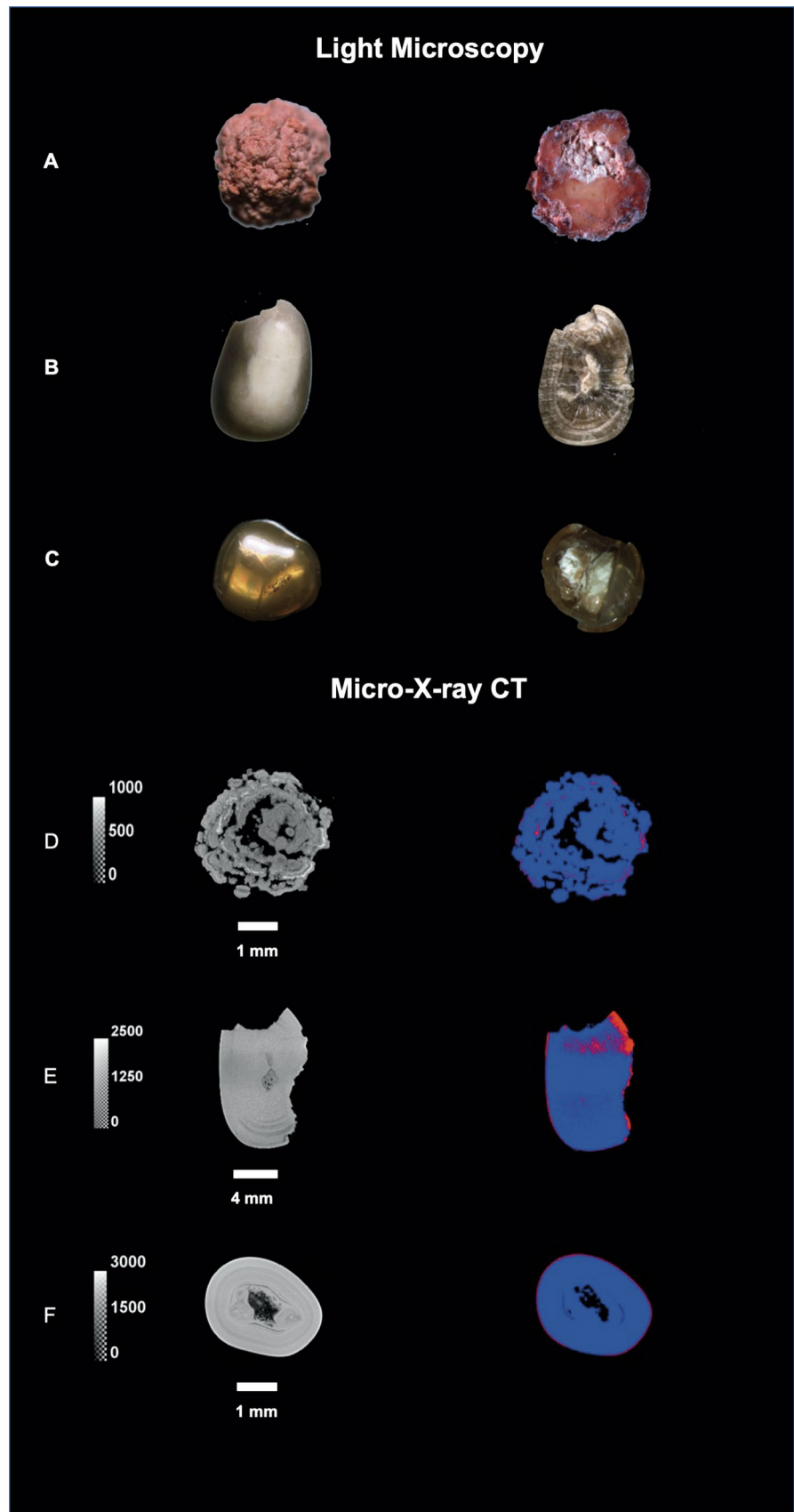


Fig. 3 Structural analyses imaged with a scanning electron microscope of Ceftriaxone stones. **a** The surface of Ceftriaxone stone was fragile and rough with large number of protruded hemispherical structures. The surface of the hemispherical structure was loose and fragile. Higher magnification illustrates honeycomb-like structure inside the spheres. **b** Arrow-like mineral edges were a part of the honeycomb-like structure (white boxes) and linked the inside architecture to the surface of the stone. **c** The higher mineral density regions of the stone (white layer in white box) illustrates many small spherical aggregates all of which were found to be adhered to the surface of the stone

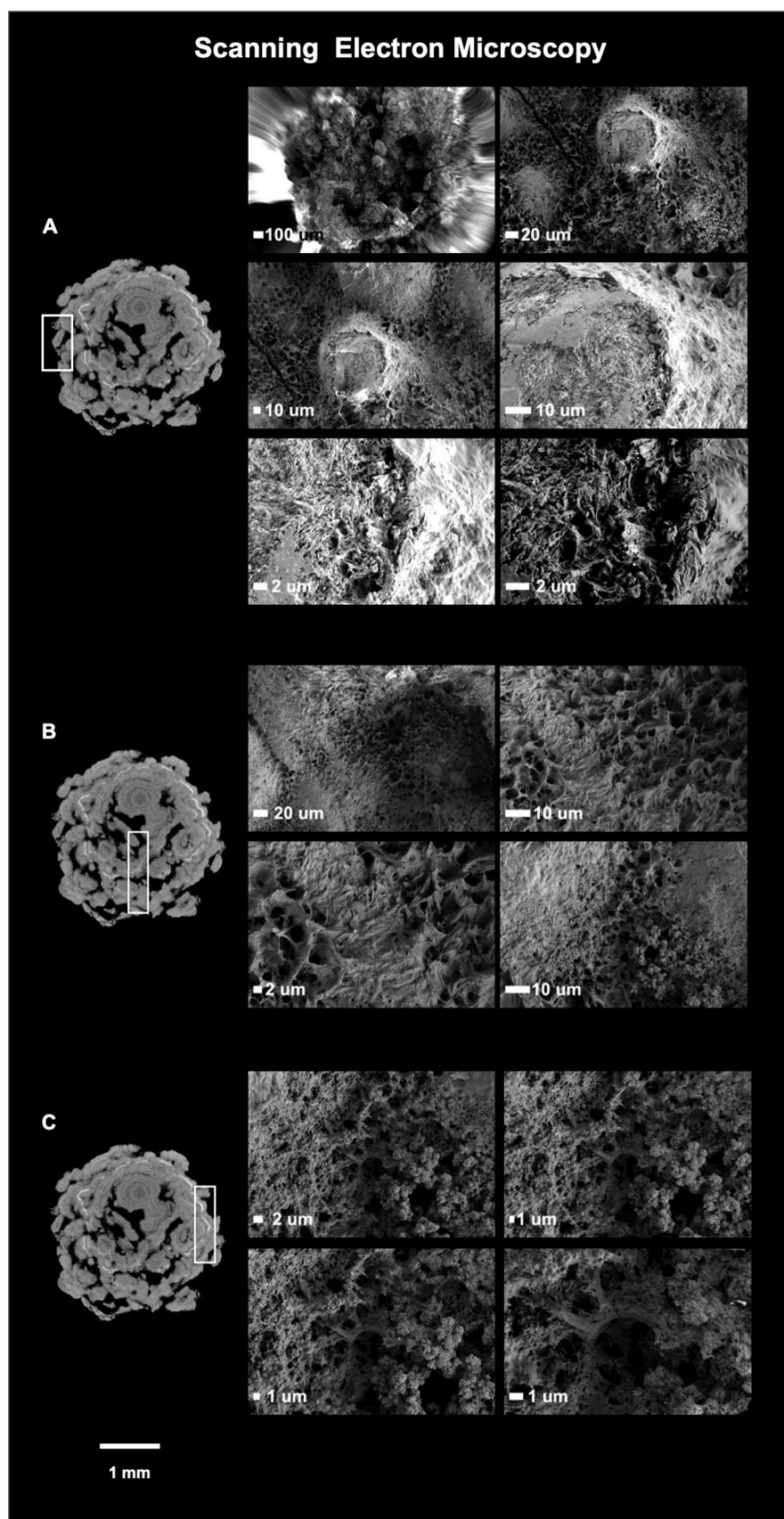


Fig. 4 Spot elemental composition analyses of Ceftriaxone stone. **a** Elemental composition of hemispherical regions on Ceftriaxone stone surface (Fig. 3a) illustrates higher sulfur and carbon. **b** Elemental composition of surface and internal regions (left of the spectra) of arrow-like minerals similar to the honeycomb structure (shown in Fig. 3b) illustrates higher sulfur and carbon. **c** Elemental composition analyses of smaller spherical regions (white layer in Fig. 3c) illustrates higher phosphorus, calcium and oxygen, while carbon percentage is reduced by half. **d** Arrow-like structure contains higher percentage of sulfur and carbon, whereas smaller spherical structure contains higher percentage of phosphorus and calcium with sodium and magnesium

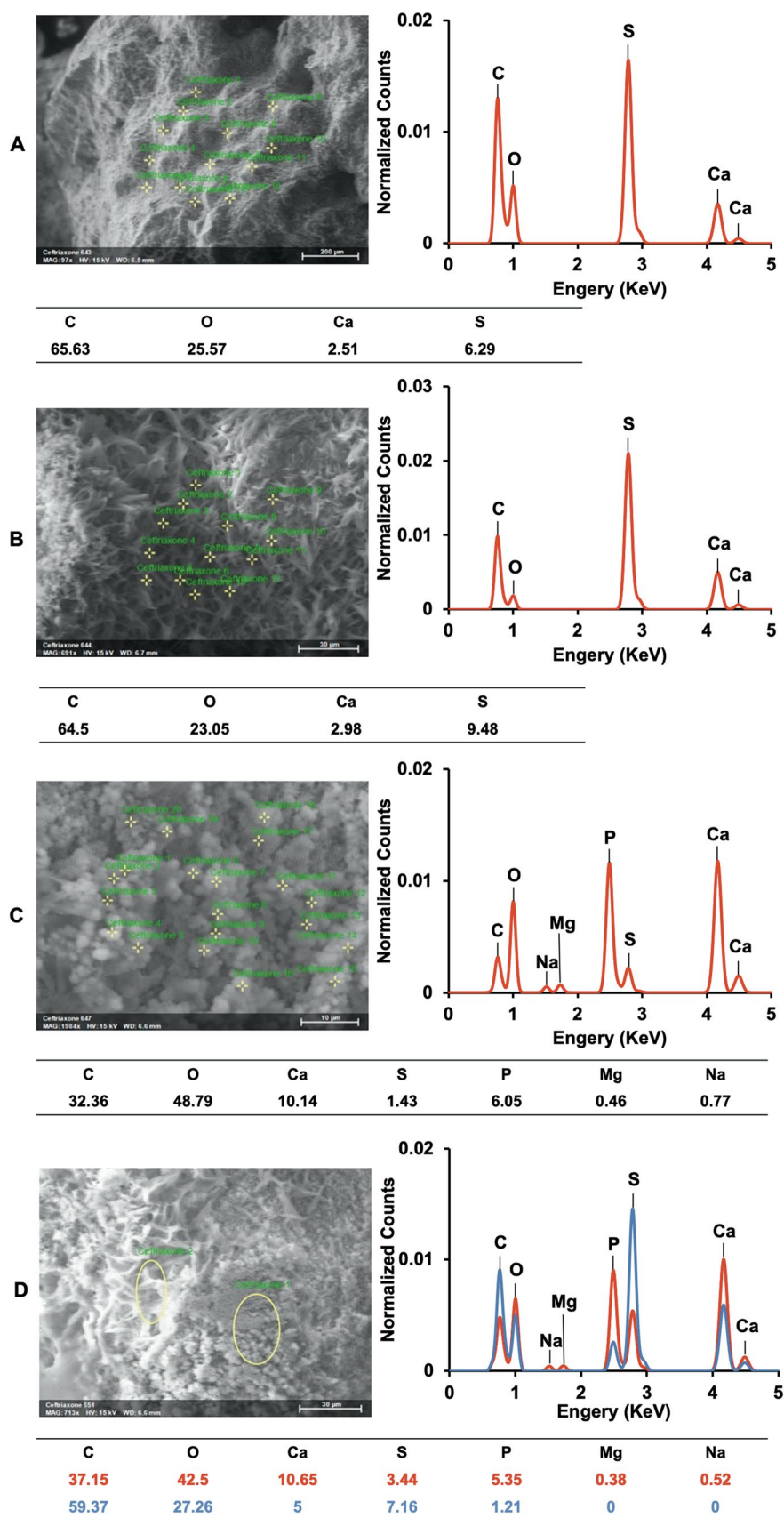
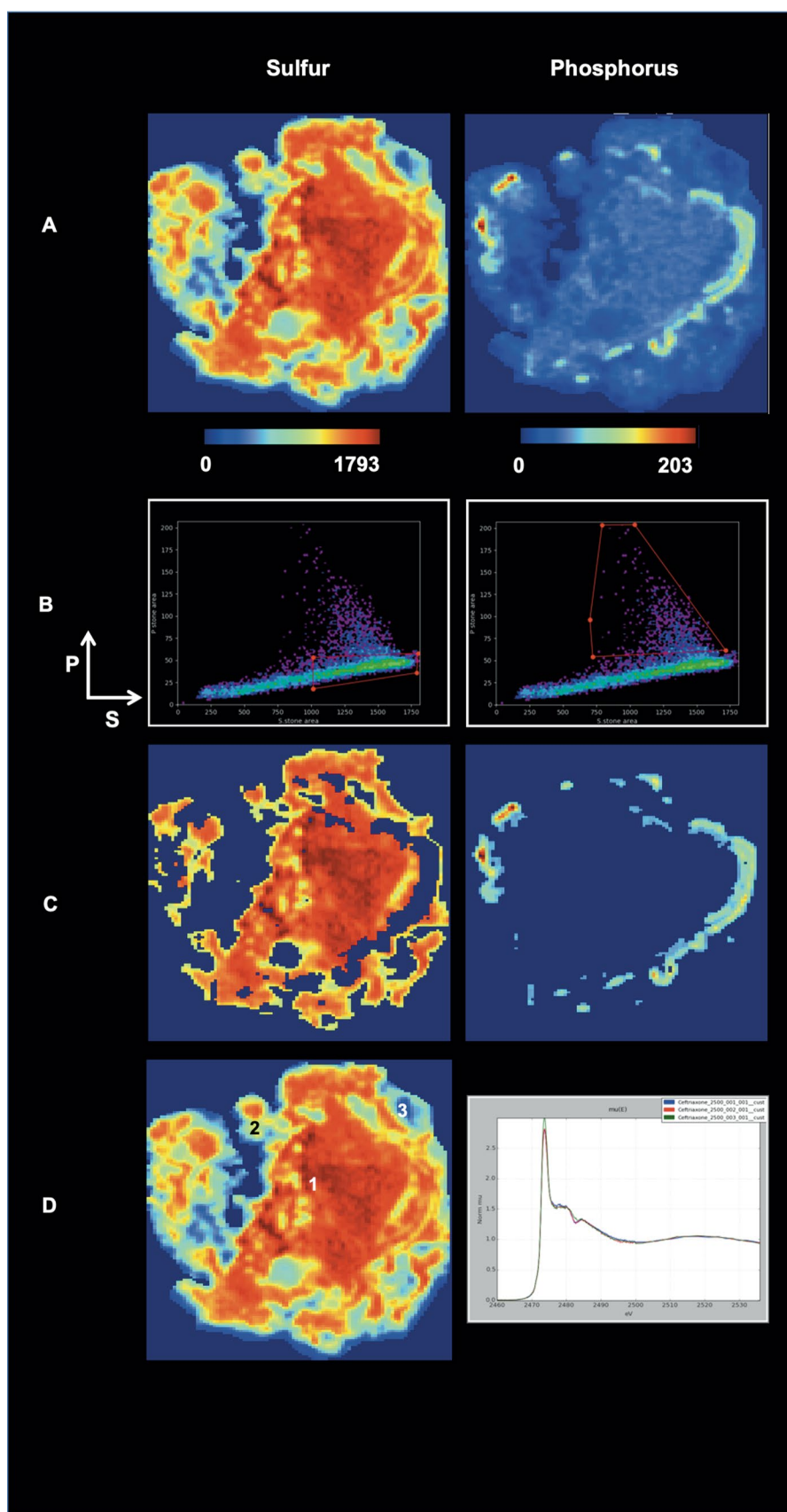


Fig. 5 Sulfur and phosphorus maps, and sulfur K-edge of Ceftriaxone using XRF microprobe and XAS. **a** Spatial distributions of sulfur (elemental counts: 0–1793) and phosphorus (0–203). **b** Scatter plots show selected regions of higher sulfur (> 1000) and phosphorus (> 50) using SMAK (Sam's Microprobe Analysis Kit). **c** Segmented higher sulfur and phosphorus regions **d** Sulfur K-edge spectra are similar at three sulfur-rich regions represented by lower (3, blue area), medium (2, green area) and higher (1, red area) sulfur contents



different spots illustrates higher, medium, and lower intensities of sulfur, and these intensities were similar (Fig. 5d) indicating same sulfur speciation between sulfur and calcium in Ceftriaxone stones.

Using light microscopy and micro-CT slices (Fig. 6a, b), the stitched yet higher resolution images obtained from SEM (Fig. 6a right) were overlaid with higher intensity sulfur and phosphorus (Fig. 6c) XRF maps by spatially correlating specific features within all the maps of the same stone. This allowed for gross geographic relationships of sulfur and phosphorus within the greater context of the structure of the stone. Spatial overlays of SEM and XRF maps and subsequent selected area EDX analyses (Fig. 7a) revealed colocalization of similar elements (Fig. 7b). These elemental maps showed two distinct phosphorus bands; calcium also showed higher intensity in the same location. Carbon and nitrogen intensity distributions were similar in the maps. Correlation of the XRF microprobe and EDX maps to specific features of the stone by SEM revealed the gross relationship between elemental to ultrastructural components of the cut yet structurally preserved Ceftriaxone specimen sections.

Discussion

Ceftriaxone, a third-generation cephalosporin with broad-spectrum gram-negative coverage is a commonly used antibiotic in pediatric patients. This drug is specifically used in developing countries because it is safe and has a long biological half-life (5–9 h). However, the solubility of Ceftriaxone is decreased when combined with calcium, and thus is more likely to form solid aggregates. Ceftriaxone also can form sludge/stone in the biliary (gallbladder) and urinary systems. Once Ceftriaxone induced stones obstruct the urinary system, placing a double J ureteral stent and bypassing the obstruction in conjunction with continued hydration resulted in stone breakage and subsequent stone passage; Ceftriaxone induced stones did not require laser or electrohydraulic lithotripsy for subsequent stone passage. Intact stone specimens used in this study were obtained from a 6-month-old infant who passed the stone after one week of Ceftriaxone treatment.

Ceftriaxone-induced sludge has been observed in the gallbladder, kidney and ureter with characteristic postacoustic shadowing seen via ultrasonography during and after Ceftriaxone treatment. Intact Ceftriaxone induced calculi are indeed rare. Ceftriaxone induced sludge and an intact Ceftriaxone induced stone passed by a 6-month-old infant were systematically collected for this study and examined in detail using correlative microscopy and spectroscopy techniques. Ceftriaxone stone mineral density was dramatically lower as compared to pediatric calcium oxalate and calcium

phosphate calculi. In addition, large amounts of voids within stones compared with routine calcium-based pediatric stones were noted; these large voids were observed in millimeter scales when investigated with micro-CT; smaller sized voids were identified in the micron-scale honeycomb structures. Loose internal stone structure with lower mineral densities were likely in part responsible for plausible disaggregation and consequent stone passage with minimal endourologic intervention. The fragile structure may be a reason that more sludge rather than intact stones are collected and have been reported.

Urinary pH and quantitative urinary citrate were factors associated with Ceftriaxone induced nephrolithiasis [8]. Potassium citrate can decrease calcium excretion in urine [9]. It is unclear how or if urinary pH and citrate accelerate Ceftriaxone induced stone formation. To better understand Ceftriaxone induced stone formation detailed stone structure studies were undertaken. Stone surface investigations with EDX revealed most areas with sulfur, carbon, oxygen, and calcium. Ceftriaxone disodium salt has three sulfurs per unit— $C_{18}H_{18}N_8Na_2O_7S_3$. The average molar ratio of sulfur to calcium is 3:1; it appears that calcium replaced the vast majority of sodium in the Ceftriaxone stone when forming calcium Ceftriaxone according to the EDX results having no sodium in the honeycomb-like structure. There were areas with unique honeycomb-like structures with associated tiny spherical structures and higher percentages of phosphorus and calcium. Magnesium and sodium were also detected in the spheres. Our results suggest that Ceftriaxone induced stones are of a combination of calcium and phosphate. Patrio et al., reported a 6-year-old patient suffered with a lower dose Ceftriaxone naturally passed out the stone as fragments following oral hydration. Infrared spectrometry revealed that the stone was composed of 90% Ceftriaxone and 10% calcium phosphate [10]. Calcium phosphate (Figs. 6b, c, 7) formed a discontinuous shell within which Ceftriaxone aggregated crystals were observed.

It is noteworthy that Ceftriaxone treatment lasted 4 days for patient with pneumonia, fever, increased respiratory rate, collectively making it difficult for the infant to feed. This relative dehydrated state of the patient reduced urine volume and likely accelerated Ceftriaxone crystal aggregation. The Ceftriaxone induced stone spontaneously passed 1 week after initiation of antibiotic therapy following which the infant's clinical situation markedly improved. Dorea and Li found that breast milk contains calcium (252 mg/L) and phosphorus (143 mg/L) and the ratio of calcium to phosphorus is 1.7 [11, 12]. During the early stages of treatment, hydration of the infant was managed with intravenous fluids and as the condition improved, the infant was able to breast feed. It is likely during breast feeding, the peak phosphate excretion was found in urine. As such, the calcium phosphate was deposited onto the surface of the rapidly forming

Fig. 6 Colocalization of sulfur and phosphorus maps using scanning electron microscopy (SEM) and X-ray fluorescence spectroscopy. **a** Ceftriaxone cross-section of stereo microscopy (left) and SEM (right) images. **b** Higher and lower mineral densities (mg/cc) are illustrated in grayscale (left) and are further delineated in blue (lower) and red (higher) mineral density regions (right). **c** Higher sulfur intensity (> 1000, left) and phosphorus (> 50, right) maps are shown in the figure. **d** Spatial overlay of structure and elemental composition specifically of stones containing higher sulfur (left) and phosphorus (right) are shown

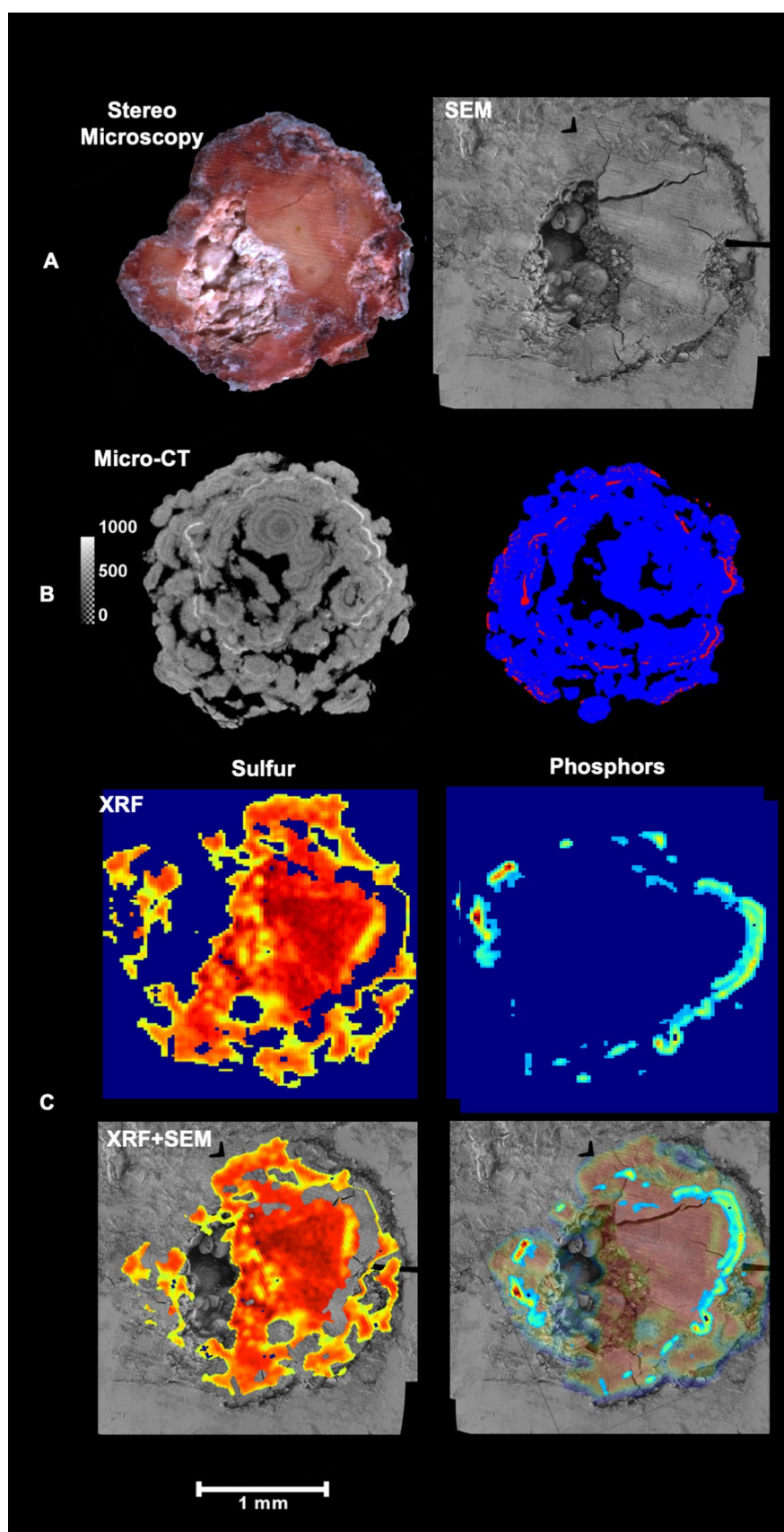
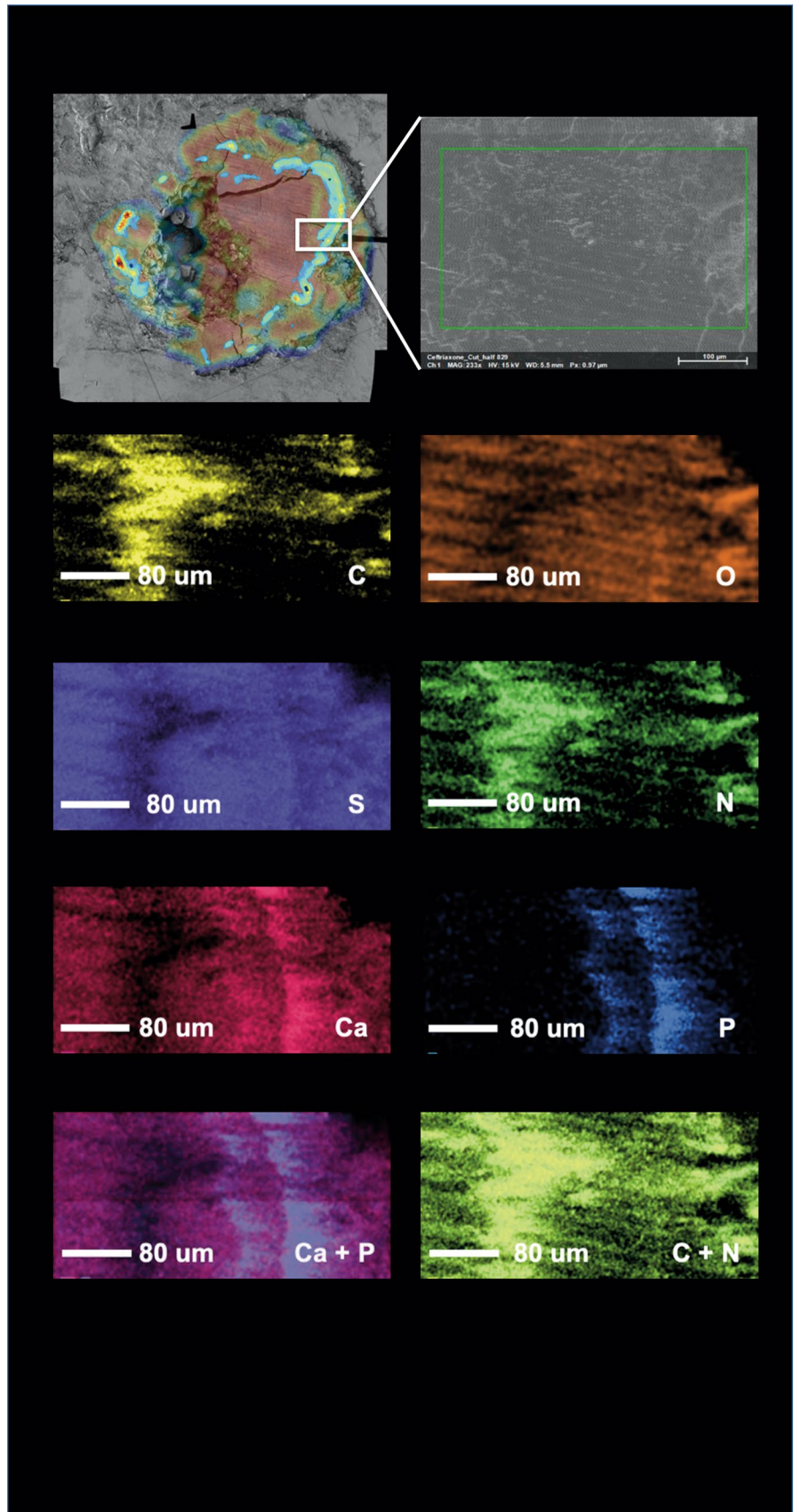


Fig. 7 Spatial maps of elements within Ceftriaxone stones using energy-dispersive X-ray spectrometer. Elemental maps localizing higher phosphorus regions (white box) in Ceftriaxone stone cross-section are shown. Higher phosphorus region also contains higher *Ca* content. *C* Carbon *O* Oxygen *S* Sulfur *N* Nitrogen *Ca* Calcium *P* Phosphorus



Ceftriaxone stone. It is interesting that we found that the calcium phosphate rings appeared in a concentric fashion on the outer area of stone. These calcium phosphate rings likely sequester and adhere to the loosely associated calcium Ceftriaxone sludge/crystals and accelerate stone formation in comparison to sludge/crystal formation.

To help better understand the mechanism of Ceftriaxone stone formations we subsequently studied Ceftriaxone induced crystal formation in vitro [Fig. 8 in Supplementary material]. Without phosphorus, Ceftriaxone combined with calcium could only form petal-like layered and cube sodium chloride crystals; these crystals were unable to aggregate to form solid stones.

Conclusion

Ceftriaxone-induced stones form rapidly and likely can be reversible by reducing urine Ceftriaxone concentration (stopping the antibiotic). Spot urine calcium and phosphate can be monitored during Ceftriaxone treatment to help reduce sludge from forming into stone material. However, once calcium and phosphate react and combine with Ceftriaxone, the sludge matures into a stone and disaggregation becomes less likely. Increased urine output and monitoring urine pH can help reduce the calcium phosphate shell that promotes rapid Ceftriaxone induced stone formation.

Research at Stanford Synchrotron Radiation Lightsource, SLAC National Accelerator Laboratory, is supported by the U.S. Department of Energy, Office of Science, Office of Basic Energy Sciences under Contract No. DE-AC02-76SF00515. The SSRL Structural Molecular Biology Program is supported by the DOE Office of Biological and Environmental Research, and by the National Institutes of Health, National Institute of General Medical Sciences (including P41GM103393). The contents of this publication are solely the responsibility of the authors and do not necessarily represent the official views of NIGMS or NIH.

Supplementary Information The online version contains supplementary material available at <https://doi.org/10.1007/s00240-020-01231-5>.

Acknowledgments This work also was supported by the National Institutes of Health: NIDCR R01 DE022032 (S.P.H.) and the Program in Biomineralization Studies (<https://sunholab.ucsf.edu/program-biomineralization-studies-PiBioms>), a joint program between the Departments of Preventive and Restorative Dental Sciences (School of Dentistry) and Urology (School of Medicine) at UCSF.

Compliance with ethical standards

Conflicts of interest There are no conflicts of interest to declare.

References

1. Patel IH, Chen S, Parsonnet M, Hackman MR, Brooks MA, Konikoff J, Kaplan SA (1981) Pharmacokinetics of ceftriaxone in humans. *Antimicrob Agents Chemother* 20(5):634–641
2. Otunctemur A, Ozbek E, Polat EC, Cekmen M, Dursun M, Cakir SS (2014) Increasing urinary calcium excretion after ceftriaxone and cephalothin therapy in adults: possible association with urolithiasis[J]. *Urolithiasis* 42(2):105–108
3. Chutipongtanate S, Thongboonkerd V (2011) Ceftriaxone crystallization and its potential role in kidney stone formation. *Biochem Biophys Res Commun* 406(3):396–402
4. Djomehri SI, Candell S, Case T, Browning A, Marshall GW, Yun W, Lau SH, Webb S, Ho SP (2015) Mineral density volume gradients in normal and diseased human tissues. *PLoS ONE* 10:e0121611. <https://doi.org/10.1371/journal.pone.0121611>
5. Sherer BA, Chen L, Yang F, Ramaswamy K, Killilea DW, Hsi RS, Stoller ML, Ho SP (2017) Heterogeneity in calcium nephrolithiasis: a materials perspective. *J Mater Res* 32:2497–2509. <https://doi.org/10.1557/jmr.2017.153>
6. Ho SP, Goodis H, Balooch M, Nonomura G, Marshall SJ, Marshall G (2004) The effect of sample preparation technique on determination of structure and nanomechanical properties of human cementum hard tissue. *Biomaterials* 25:4847–4857
7. Sherer BA, Chen L, Kang M et al (2018) A continuum of mineralization from human renal pyramid to stones on stems[J]. *Acta Biomater* 71:72–85
8. Cong X, Gu X, Sun X, Ning B, Shen L (2014) Possible function of urinary pH and citrate on the ceftriaxone-induced nephrolithiasis. *Urology* 83(1):63–67
9. Song Y, Hernandez N, Shoag J, Goldfarb DS, Eisner BH (2016) Potassium citrate decreases urine calcium excretion in patients with hypocitraturic calcium oxalate nephrolithiasis[J]. *Urolithiasis* 44(2):145–148
10. Gargollo PC, Barnewolt CE, Diamond DA (2005) Pediatric ceftriaxone nephrolithiasis. *J Urol* 173(2):577–578
11. Dorea JG (1999) Calcium and phosphorus in human milk. *Nutr Res* 19(5):709–739
12. Li C, Solomons NW, Scott ME, Koski KG (2016) Minerals and trace elements in human breast milk are associated with Guatemalan infant anthropometric outcomes within the first 6 months. *J Nutr* 146(10):2067–2074

Publisher's Note Springer Nature remains neutral with regard to jurisdictional claims in published maps and institutional affiliations.